NASA TECHNICAL NOTE

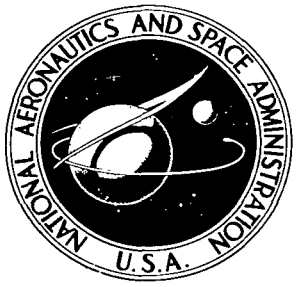

NASA TN D-5176

C.1

NASA TN D-5176

ON SOME NUMERICAL DIFFICULTIES IN INTEGRATING THE EQUATIONS FOR ONE-DIMENSIONAL NONEQUILIBRIUM NOZZLE FLOW

by Harvard Lomax, Harry E. Bailey, and Franklyn B. Fuller

Ames Research Center
Moffett Field, Calif.

NATIONAL AERONAUTICS AND SPACE ADMINISTRATION • WASHINGTON, D. C. • APRIL 1969

ON SOME NUMERICAL DIFFICULTIES IN INTEGRATING THE EQUATIONS FOR ONE-DIMENSIONAL NONEQUILIBRIUM NOZZLE FLOW

By Harvard Lomax, Harry E. Bailey,
and Franklyn B. Fuller

Ames Research Center
Moffett Field, Calif.

NATIONAL AERONAUTICS AND SPACE ADMINISTRATION

For sale by the Clearinghouse for Federal Scientific and Technical Information
Springfield, Virginia 22151 – CFSTI price $3.00

ON SOME NUMERICAL DIFFICULTIES IN INTEGRATING THE EQUATIONS FOR ONE-DIMENSIONAL NONEQUILIBRIUM NOZZLE FLOW

By Harvard Lomax, Harry E. Bailey,
and Franklyn B. Fuller

Ames Research Center

SUMMARY

Several numerical difficulties arise in the problem of integrating the ordinary differential equations that represent the flow of a gas in chemical nonequilibrium through a nozzle. These difficulties are identified with parasitic eigenvalues, saddle-point behavior, and indeterminate forms. The numerical difficulties and the methods that successfully overcame them for the particular examples analyzed are discussed in this report.

INTRODUCTION

The equations representing one-dimensional steady flow of a gas in chemical equilibrium through a nozzle (channel flow) are well known (see, e.g., ref. 1). These equations are treated again here for the purpose of studying certain difficulties, specifically, saddle-point behavior, that arise when they are integrated numerically through the transonic region. The technique developed from the simpler problem is then applied to clarify some of the difficulties encountered in integrating the much more complicated equations that represent the flow through a nozzle of a gas in nonequilibrium. The physical model of air used in these computations is the same as that used in reference 2. This model has been greatly improved in the ensuing years in a variety of ways by a variety of authors. However, this report is an analysis of numerical difficulties that can arise in integrating the equations formed from the choice of any model, and, for this purpose, the one chosen appears reasonably representative.

In reference 2, a critical analysis of several numerical methods for computing the flow of a gas in chemical nonequilibrium has been carried out. Certain information contained in that reference, such as the concept of parasitic eigenvalues and the construction and value of implicit methods, is helpful for a detailed understanding of the material presented here. However, in reference 2, the examples are limited to the nonequilibrium flow behind a normal shock wave. Additional complications arise in the transonic section of a nozzle; two of the most important are those arising from the existence of a saddle point and the problem of numerical solution of the differential equations when the gas they represent is nearly in equilibrium.

The question of integrating through the saddle point has generally been avoided by considering the gas to be in equilibrium from a position upstream of the minimum section to one a little downstream from it. In fact, most often a pressure distribution along the channel is assumed in this region; the corresponding cross-sectional area follows from a direct calculation, and a few iterations produce the desired approximate nozzle shape in the transonic part. This procedure is not always usable, however, and, in this report, direct methods are developed for treating saddle points. For example, if the flow is out of equilibrium upstream of the throat, the abovementioned device is unsatisfactory. An example of such a case is included here. Also, in other problems, such as blunt-body flow, the method of integral relations often leads to saddle-point behavior, and it becomes necessary to use techniques such as those to be presented.

SYMBOLS

$[\ ]$	matrix of enclosed quantity
$[\ ]^{-1}$	inverse of matrix
$\bar{A}$	cross-sectional area of nozzle
$\bar{A}_x$	derivative of $\bar{A}$ with respect to x
$[A_n]$	matrix in locally linearized equations (see eq. (10))
a	equilibrium speed of sound
a^*	critical speed of sound
$\left(a_{ij}\right)_n$	element in A_n matrix
c_p^*	$\sum_i \gamma_i c_{p_i}$
c_{p_i}	specific heat at constant pressure for ith species
er_λ	truncation error
F	derivative of w with respect to s (see eq. (6))
h	step size
h_i	enthalpy of ith species
$[I]$	unit matrix
n	step number

p pressure

Q^i production of species i in moles per unit volume per unit time

R universal gas constant

s independent variable

s_o scale factor (see eqs. (3))

T temperature

u velocity

w dependent variable in coupled equations (see eq. (6))

x distance along nozzle

z^* $\sum_i \gamma_i$

γ ratio of specific heats for a perfect gas

γ_i molar concentration of ith species, moles/gm

ρ density

σ eigenvalue of matrix $[A_n]$

Superscripts

$\rightarrow$ vector

T transpose of vector

$'$ differentiation with respect to s

BASIC EQUATIONS

Equilibrium Flow

When an inviscid channel flow is in chemical equilibrium, the basic equations can be expressed in terms of the three dependent variables u, ρ, and p by the matrix equation

$$\begin{bmatrix} \rho\bar{A} & u\bar{A} & 0 \\ \rho u & 0 & 1 \\ 0 & -a^2 & 1 \end{bmatrix} \begin{bmatrix} u_x \\ \rho_x \\ p_x \end{bmatrix} = \begin{bmatrix} -\rho u\bar{A}_x \\ 0 \\ 0 \end{bmatrix} \tag{1}$$

where x is the independent variable representing length along the channel, $\bar{A}$ is the channel cross-sectional area at a given x, and the subscript indicates differentiation with respect to x. It is well known that the solution of equation (1) can be found directly, and the dependent variables u, p, and ρ can be expressed as functions of $\bar{A}$ and reference conditions (see, e.g., ref. 1). As was pointed out in the Introduction, however, we are interested here in the numerical solution of equation (1) in order to study the techniques required to treat more complicated problems with fundamentally similar numerical difficulties that cannot be resolved analytically.

Equation (1) can be solved directly for the derivative terms. One finds

$$\left.\begin{aligned} u_x &= -\frac{ua^2\bar{A}_x}{\bar{A}(a^2 - u^2)} \\ \rho_x &= \frac{\rho u^2\bar{A}_x}{\bar{A}(a^2 - u^2)} \\ p_x &= \frac{\rho u^2 a^2\bar{A}_x}{\bar{A}(a^2 - u^2)} \end{aligned}\right\} \tag{2}$$

which give, by inspection, the well-known condition that if the velocity becomes sonic, the derivatives of the dependent variables all have zero denominators; if they are to remain continuous, the numerators must also vanish. In this case, the numerators can vanish only if $\bar{A}_x = 0$, which leads to the well-known fact that the sonic velocity occurs at the throat. Of principal interest for our purposes is the fact that this indeterminate form leads to the study of critical points (in particular, saddle points) and the numerical difficulties that occur near them.

An analysis of saddle points from a numerical standpoint is presented in the next part. Now we note only that the indeterminacy in equations (2) can be eliminated by a simple transformation; the general procedure is outlined in reference 2. Introducing the new independent variable s, defined by

$$x' \equiv \frac{dx}{ds} = s_o\bar{A}(a^2 - u^2)$$

where s_o is a constant scale factor, makes x a dependent variable in the new set of four coupled nonlinear differential equations

$$u' = \frac{du}{ds} = -s_o ua^2\bar{A}_x \tag{3a}$$

$$\rho' = s_o\rho u^2\bar{A}_x \tag{3b}$$

$$p' = s_o\rho u^2 a^2\bar{A}_x \tag{3c}$$

$$x' = s_o\bar{A}(a^2 - u^2) \tag{3d}$$

Notice that equations (3) are determinate for all finite values of s and autonomous (i.e., s does not appear explicitly on the right-hand sides of the equations).

Nonequilibrium Flow

The basic equations used herein for nonequilibrium channel flow are identical to those presented as equations (1) in reference 2. With a slight change in the notation (z^* for $\sum_i \gamma_i$, C_p^* for $\sum_i \gamma_i c_{p_i}$), the equations can be written

$$\left.\begin{aligned}
\rho\bar{A}\frac{du}{dx} + u\bar{A}\frac{d\rho}{dx} &= -\rho u\bar{A}_x \\
\rho u\frac{du}{dx} + Rz^*T\frac{d\rho}{dx} + \rho Rz^*\frac{dT}{dx} + \rho RT\sum_1^N \frac{d\gamma_i}{dx} &= 0 \\
u\frac{du}{dx} + C_p^*\frac{dT}{dx} + \sum_1^N h_i\frac{d\gamma_i}{dx} &= 0 \\
\rho u\frac{d\gamma_1}{dx} &= Q^1(\rho,T,\gamma_1,\ \ldots,\ \gamma_N) \\
&\ \ \vdots \\
\rho u\frac{d\gamma_N}{dx} &= Q^N(\rho,T,\gamma_1,\ \ldots,\ \gamma_N)
\end{aligned}\right\} \quad (4)$$

If equations (4) are solved for the derivatives du/dx, $d\rho/dx$, and dT/dx, each expression has in its denominator the term

$$TRz^*C_p^* - u^2(C_p^* - Rz^*)$$

which is the counterpart of the term $a^2 - u^2$ that appeared in equations (2). It can be eliminated by a transformation similar to equation (3d). There results

$$
\left.
\begin{aligned}
u' \equiv \frac{du}{ds} &= s_o \rho u R \bar{A}\left[-z^* D_1 + C_p^* T D_2 \right] - R z^* T \rho u^2 C_p^* \bar{A}_x \\
\rho' &= s_o \rho^2 R \bar{A}\left[z^* D_1 - C_p^* T D_2 \right] + \rho^2 u^3 \left(C_p^* - R z^* \right) \bar{A}_x \\
T' &= s_o \rho \bar{A}\left[(u^2 - R z^* T) D_1 - u^2 \rho R T D_2 \right] + R z^* T \rho u^3 \bar{A}_x \\
x' &= s_o \rho u \bar{A}\left[T R z^* C_p^* - u^2 \left(C_p^* - R z^* \right) \right] \\
\gamma_i' &= s_o \rho \bar{A} Q^i \left[T R z^* C_p^* - u^2 \left(C_p^* - R z^* \right) \right], \qquad i = 1, \ldots, N
\end{aligned}
\right\} \tag{5}
$$

where

$$
D_1 = \sum_1^N h_i Q^i
$$

$$
D_2 = \sum_1^N Q^i
$$

and where s_o is again a scale constant. The dependent variable T has replaced p, used in the equilibrium case, and the N species concentrations are now coupled into the equations. Notice, however, that the equations are determinate and autonomous.

Some of the numerical difficulties that occur in integrating equations (5) can be illustrated by a study of the much simpler equations (3). Hence, the first part of the report will be devoted to the numerical analysis of equilibrium flow.

Local Linearization

The locally linearized forms of equations (3) and (5) will next be constructed, following the procedure of reference 2. In either case, equilibrium or nonequilibrium, the equations of motion can be represented in vector notation as

$$
\vec{w}' \equiv \frac{d\vec{w}}{ds} = \vec{F}(\vec{w}) \tag{6}
$$

where, for equations (3),

$$
\vec{w}^T = (u, \rho, p, x) \tag{7}
$$

and for equations (5)

$$\vec{w}^T = (u,\rho,T,\gamma_1, \ldots, \gamma_N,x) \tag{8}$$

Note that equations (6) are quasi-linear, that is, the highest derivative appears linearly. The linearization is now performed by expansion of each component of the vector $\vec{F}$, denoted F_i, in a multidimensional Taylor series about the point $s_n = nh$. This gives, after substituting equation (6),

$$\vec{w}_i' = F_{in} + (w_1 - w_{1n})\left(\frac{\partial F_i}{\partial w_1}\right)_n + \ldots + (w_m - w_{mn})\left(\frac{\partial F_i}{\partial w_m}\right)_n + O\left[|\vec{w} - \vec{w}_n|^2\right] \tag{9}$$

for the ith component w_i' of w'. The number of components of $\vec{w}$ is taken to be m; hence, there are m coupled equations such as (9) in the set. Note that when $\vec{w} = \vec{w}(s + nh) = \vec{w}_{n+1}$

$$|\vec{w} - \vec{w}_n|^2 = |\vec{w}_{n+1} - \vec{w}_n|^2 = h^2|\vec{w}_n'|^2 + O(h^3)$$

by Taylor expansion. By defining the Jacobian matrix

$$[A] = (a_{ij}) = \left(\frac{\partial F_i}{\partial w_j}\right)$$

the set of equations (6) can be written

$$\vec{w}' = \vec{F}_n + [A_n](\vec{w} - \vec{w}_n) + O(h^2)$$

$$= [A_n]\vec{w} + \vec{f}_n + O(h^2) \tag{10}$$

where

$$\vec{f}_n = \vec{F}_n - [A_n]\vec{w}_n \tag{11}$$

It is important that although equation (10) represents the local linearization of equation (6) (referenced to $s_n = nh$), it is the derivative $\vec{w}'$ that is represented as linear in the stepsize h. Therefore, in a differencing scheme, the linearization here is consistent with any method that approximates the function itself with a second-degree polynomial. For example, if the difference scheme is

$$\vec{w}_{n+1} = \vec{w}_n + \frac{1}{2}h(\vec{w}_{n+1}' + \vec{w}_n') + O(h^3)$$

then inserting expression (10) for the derivative terms does not alter the order of the error.

The [A] matrix is not difficult to construct analytically in the case of equilibrium flow represented by equation (3). It is especially simple (and just as instructive) to assume a calorically perfect gas; then

$$a^2 = \frac{\gamma p}{\rho}, \qquad \frac{\partial a^2}{\partial \rho} = -\frac{a^2}{\rho}, \qquad \frac{\partial a^2}{\partial p} = \frac{a^2}{p}$$

and

$$[A] = \begin{bmatrix} -s_o a^2 \bar{A}_x & s_o \frac{1}{\rho} u a^2 \bar{A}_x & -s_o \frac{1}{p} u a^2 \bar{A}_x & -s_o u a^2 \bar{A}_{xx} \\ 2 s_o \rho u \bar{A}_x & s_o u^2 \bar{A}_x & 0 & s_o \rho u^2 \bar{A}_{xx} \\ 2 s_o \rho u a^2 \bar{A}_x & 0 & s_o \frac{1}{p} \rho u^2 a^2 \bar{A}_x & s_o \rho u^2 a^2 \bar{A}_{xx} \\ -2 s_o u \bar{A} & -s_o \frac{1}{\rho} a^2 \bar{A} & s_o \frac{1}{p} a^2 \bar{A} & s_o (a^2 - u^2) \bar{A}_x \end{bmatrix} \tag{12}$$

If the nonequilibrium equations (4) are to be integrated by means of implicit formulas, the A matrix will be 13 × 13 for the gas model used in reference 2 and in the present report. However, just as in reference 2, the elements of A are not determined analytically. They are computed by the approximate formula

$$\frac{\partial F_i}{\partial w_j} \approx \frac{F_i(1.01 w_j) - F_i(0.99 w_j)}{0.02 w_j} \tag{13}$$

NUMERICAL INTEGRATION THROUGH A SADDLE POINT

Introductory Example

The analytical behavior of autonomous systems of first-order ordinary differential equations has been thoroughly studied in the mathematical literature. The facet of this material of particular interest in the present investigation is well summarized in reference 3, page 70, ff. As mentioned previously, this part of the theory is the study of behavior of solutions near a critical point, specifically, a critical point of the type known as a saddle

point. Because of the advantage of geometrical visualization of the points involved, the case involving only two independent variables will be considered first.

Let there be two differential equations

$$\left.\begin{aligned} \frac{dx}{dt} &= P(x,w) \\ \frac{dw}{dt} &= Q(x,w) \end{aligned}\right\} \tag{14}$$

which can be put in the form

$$\left.\begin{aligned} \frac{dx}{dt} &= a_{11}x + a_{12}w + f_1(x,w) \\ \frac{dw}{dt} &= a_{21}x + a_{22}w + f_2(x,w) \end{aligned}\right\} \tag{14a}$$

Further, suppose that $a_{11}a_{22} - a_{21}a_{22} \neq 0$, and that

$$\lim_{x,w \to 0} \frac{f_i}{\sqrt{x^2 + w^2}} = 0 , \qquad i = 1, 2 \tag{14b}$$

The point $x = w = 0$ is then said to be a simple singularity of the system. It is shown in the theory (see, e.g., ref. 3) that under such circumstances, the singularity of system (14) at $x = w = 0$ has essentially the same nature as that of the linearized system

$$\left.\begin{aligned} \frac{dx}{dt} &= a_{11}x + a_{12}w \\ \frac{dw}{dt} &= a_{21}x + a_{22}w \end{aligned}\right\} \tag{15}$$

The constants a_{ij} are components of the Jacobian matrix used above, that is,

$$a_{11} = \left(\frac{\partial P}{\partial x}\right)_{x=w=0} , \ \ldots , \ a_{22} = \left(\frac{\partial Q}{\partial w}\right)_{x=w=0}$$

Hence the condition on the constants a_{ij} can be stated in terms of the non-vanishing of the Jacobian $\partial(P,Q)/\partial(x,w)$ at the origin.

Note that in this case the differential equations (15) can be combined to give

$$\frac{dx}{dw} = \frac{a_{11}x + a_{12}w}{a_{21}x + a_{22}w}$$

The point $x = w = 0$ is then seen to be one at which the derivative is indeterminate. While this simple means serves to fix the saddle point when there are two variables involved, such as x and w above, it is not clear at once how it can be extended to more complicated cases, such as that represented by the system of equations (5). A more suitable test for more than two variables is given below.

As an example, consider the autonomous linear system of differential equations:

$$\left.\begin{aligned} \frac{dw}{ds} &= 2w - x + 0.5 \\ \frac{dx}{ds} &= -w \qquad + 1.0 \end{aligned}\right\} \tag{16}$$

or

$$\frac{dw}{dx} = \frac{2w - x + 0.5}{1 - w} \tag{16a}$$

From the latter form it is seen that the critical point is at $w = 1$, $x = 2.5$. It is helpful to put equations (16) into the vector-matrix notation used above in the section on Local Linearization. Thus, put

$$\vec{w}^T = (w,x); \qquad [A] = \begin{bmatrix} 2.0 & -1.0 \\ 1.0 & 0 \end{bmatrix}; \qquad \vec{f}^T = (0.5,1.0)$$

and equations (16) can be written

$$\vec{w}' = [A]\vec{w} + \vec{f} \tag{16b}$$

This equation is formally equivalent to the linearized form, that is, that obtained by neglecting terms $O(h^2)$ in equation (10).

The eigenvalues of the matrix in equation (16b) are

$$\left.\begin{aligned} \sigma_1 &= 1 - \sqrt{2} \approx -0.414 \\ \sigma_2 &= 1 + \sqrt{2} \approx \ \ 2.414 \end{aligned}\right\} \tag{17}$$

They are real and of opposite sign. This fact is important since it characterizes, for the two-dimensional case, the critical point as a saddle point. In cases where more variables are present, the presence of eigenvalues of different sign, in company with a requirement that solutions remain finite, can be taken as indications of saddle-type behavior. The behavior of the integral curves of equation (16a) (or (16b)) is easily found. Independent solutions for w and x are combinations of the complementary solutions $e^{\sigma_1 s}$ and $e^{\sigma_2 s}$ with the particular integral $w = 1.0$, $x = 2.5$. If w_o and x_o are the values of w and x, respectively, at $s = 0$, then the general solution of equation (16b) is

$$
\left.
\begin{aligned}
w - 1.0 &= \frac{1}{2\sqrt{2}}\left[(x_o - 2.5) - \sigma_1(w_o - 1)\right]e^{\sigma_1 s} \\
&\quad - \frac{1}{2\sqrt{2}}\left[(x_o - 2.5) - \sigma_2(w_o - 1)\right]e^{\sigma_2 s} \\
x - 2.5 &= \frac{\sigma_2}{2\sqrt{2}}\left[(x_o - 2.5) - \sigma_1(w_o - 1)\right]e^{\sigma_1 s} \\
&\quad - \frac{\sigma_1}{2\sqrt{2}}\left[(x_o - 2.5) - \sigma_2(w_o - 1)\right]e^{\sigma_2 s}
\end{aligned}
\right\} \qquad (18)
$$

Since σ_1 and σ_2 are real and of opposite sign, with $\sigma_2 > 0$, it is clear that one or the other of the exponential terms must have a zero coefficient if a solution is to remain finite as $s \to \pm\infty$. Thus, a finite solution as $s \to +\infty$ results if $x_o - 2.5 = \sigma_2(w_o - 1)$ while a finite solution as $s \to -\infty$ results if $x_o - 2.5 = \sigma_1(w_o - 1)$. In these two cases, the integral curves are contained in the lines (separatrices)

$$w - 1 = \frac{1}{\sigma_2}(x - 2.5) \qquad (19a)$$

$$w - 1 = \frac{1}{\sigma_1}(x - 2.5) \qquad (19b)$$

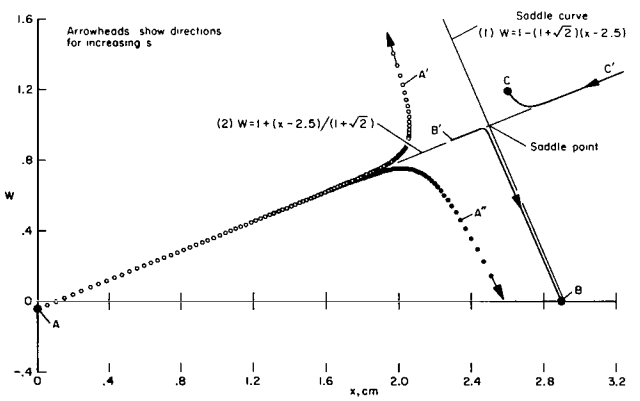

Sketch (a).- Saddle curve behavior for equations (16).

respectively. These lines are identified in sketch (a).

If the initial conditions (x_o, w_o) lie on line (2) in the sketch, then as s increases the solution will follow this line toward the point (2.5, 1.0). Integration in the opposite direction (s decreasing) would give an integral curve moving away from the saddle point. Similar remarks, with sign reversal on s, hold for the line (1) in the sketch.

If the initial conditions do not satisfy one of equations (19), no matter how small the error, the corresponding integral curve will contain an exponentially increasing component that will prevent the curve from ever approaching the saddle point. Instead, the curve will have a hyperbola-like shape and will ultimately approach $\pm\infty$. This fact is at the root of numerical difficulties in the solution of differential equations having saddle-point singularities; since computing machines do not reproduce numbers exactly, there will always be an error in the initial conditions.

We shall now discuss the numerical determination of the integral curves of equation (16b). The particular method chosen is the second-order Runge-Kutta:

$$\left.\begin{aligned} u_{n+1}^{(1)} &= u_n + hu_n' \\ u_{n+1} &= u_n + \frac{1}{2}h\left(u_{n+1}^{(1)\prime} + u_n'\right) \end{aligned}\right\} \tag{20}$$

This method will also be used later in integrating the flow equations discussed in the previous sections. Precise meanings of terms and symbols used in equations (20) and the numerical analysis that follows can be found in references 4 and 5.

Accuracy

The accuracy of the integral curves found by applying the integration method (20) to the differential equations (16) will be discussed first. The truncation error, er_λ, for the second-order Runge-Kutta method is given by (see ref. 5, p. 63)

$$er_\lambda = \frac{1}{6}(\sigma h)^3$$

Here, $\sigma = \sigma_2 = 2.41$ is the largest eigenvalue. Hence, a stepsize $h = \Delta s = 0.05$ gives a local truncation error of about

$$er_\lambda = 3\times10^{-4}$$

Thus, we should expect a total accumulated ("global") error of less than 3 percent after 100 steps. This expectation is borne out by comparison of the calculated solution with the exact one. The results (which correspond to curves AA' and AA'' in sketch (a)) are listed below (note that the initial conditions were chosen to lie above and below the separatrix by approximately equal amounts).

TABLE I

Curve	Initial values		Numerical results after 100 steps		Exact results for same s	
	w_o	x_o	w	x	w	x
AA'	-0.035531	0	1.2411	2.0232	1.2516	2.0189
AA''	-0.035537	0	.4686	2.3413	.4595	2.3470

The point to be made here is that the numerical method (20) is sufficiently accurate, that is, increasing the accuracy of numerical integration would not lead to discernibly different results to the scale of sketch (a).

Instabilities

Induced instability.- The real stability boundary of the Runge-Kutta method given by equation (20) is -2.0 (ref. 5, p. 83). That is, in the present case, h is limited to the range

$$|\sigma h| < 2$$

where σ is the largest negative eigenvalue of the matrix [A] in equation (16b). This value is $\sigma_1 = -0.414$, so that h can be as large as 4.8 without bringing on the induced instability. If the direction of integration were reversed, the largest negative eigenvalue would become $-\sigma_2 = -2.41$, and there would be no induced instability for $h < 0.83$. Hence, for the present problem, there is absolutely no danger of induced instability with the stepsize $h = 0.05$ used.

Inherent instability.- From the above discussion, it is seen that there is actually no numerical difficulty, either in regard to accuracy or to induced instability, in calculating the integral curves marked AA' and AA'' in sketch (a), the initial values for which are given in table I. Thus, if such a result is indeed the correct answer for the problem set, there is no more to be said. However, it is usually the case that when a saddle point occurs in a problem the desired result for the integral curve is the separatrix or saddle curve. As we have seen from the example above (sketch (a)), reaching the saddle point by forward integration from a given initial position is difficult indeed. For the case examined above, the initial conditions for a point on the saddle line starting at $x = 0$ are

$$x_o = 0, \qquad w_o = \frac{1}{2}(7 - 5\sqrt{2})$$

Since the computer is unable to represent exactly the number $\sqrt{2}$, it is impossible to exclude completely terms in $e^{\sigma_2 s} = e^{(1+\sqrt{2})s}$ from the solution (s increasing).

This is an example of an inherent instability (ref. 4, p. 48). That is, it is not possible to exclude from the numerical solution the terms in equations (18) that contain the growing exponential, $e^{\sigma_2 s} = e^{2.414s}$. Again, this occurs because an irrational number cannot be represented exactly on a binary digital computer.

In summary

1. There is no numerical difficulty per se, either with regard to accuracy or stability, in numerically evaluating integral curves in the "vicinity" of a saddle curve. (The precise definition of vicinity is governed by the word length of the particular computer used for the computation.)

2. The saddle curve itself is inherently unstable and its numerical calculation involves all the difficulties associated with such an instability.

Numerical Integration Through Saddle Points

General dicussion.- Actually, the numerical integration of saddle curves may or may not lead to difficulty. Recall that, by definition, a saddle point can occur only if there are two real eigenvalues of opposite sign in the [A] matrix of the coupled equations. No matter in what direction the integration proceeds, therefore, there is always a positive eigenvalue in the presence of a negative one; and, again by definition, an inherent instability exists if that particular solution is desired for which all effects of the positive eigenvalue disappear from the exact analysis. We now show that the numerical difficulties depend upon the ratio of these two eigenvalues and the direction of integration when their magnitudes are unequal.

Consider equations (15). Transform, by an appropriate rotation and displacement, to a new set of variables, y_1 and y_2, that lie along the saddle curves, with origin at the saddle point itself (as shown in sketch (b)). This transformation uncouples equations (15) and we find solutions in the form

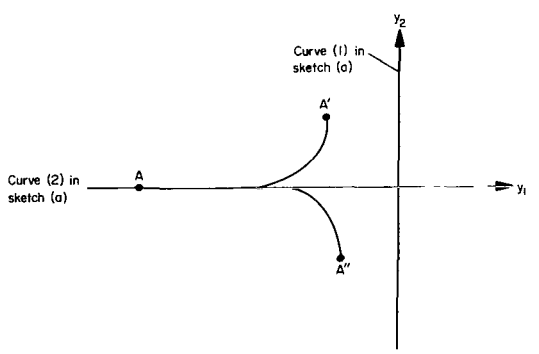

Sketch (b)

$$\left.\begin{aligned} y_1(s) &= y_1(0)e^{\sigma_1 s} \\ y_2(s) &= y_2(0)e^{\sigma_2 s} \end{aligned}\right\} \qquad (21)$$

The parameter s can be eliminated from these equations, leading to the solution

$$\left[\frac{y_1(s)}{y_1(0)}\right]^{1/\sigma_1} = \left[\frac{y_2(s)}{y_2(0)}\right]^{1/\sigma_2} \qquad (22)$$

Now if y_1 is started a distance -2.5 units from the origin (saddle point) and y_2 a distance ϵ above the y_1 axis, we have

$$y_1(s) = -2.5\left[\frac{1}{\epsilon}\, y_2(s)\right]^{\sigma_1/\sigma_2}$$

If we proceed to integrate (accurately) to where $y_2 = 1$, there results

$$y_1 = -2.5\left(\frac{1}{\epsilon}\right)^{(1-\sqrt{2})/(1+\sqrt{2})} = -2.5\epsilon^{0.171}$$

Even if ϵ had been chosen as small as 10^{-6}, y_1 would still be -0.223 units from the y_2 axis after the integration. This accounts for the divergence from the separatrix of curves AA' and AA'' in sketch (a).

Next, notice that if conditions are reversed and one starts with ($y_1 = \epsilon$, $y_2 = -2.5$) and proceeds to integrate until $y_1 = 1$, the results would be

$$y_2 = -2.5\epsilon^{5.83}$$

This leads to a behavior quite different from that encountered in integrating from A to A'. To illustrate this, integration of equations (16) was started at point B in sketch (a), and integrated (using eqs. (20) with $\Delta s = -0.05$) for 140 steps. The results are given by the solid line BB' in the sketch, and the initial and final values are presented in table II.

TABLE II

Curve	Initial values		Numerical results after 140 steps		Exact results for same s	
	w	x	w	x	w	x
BB'	0	2.9	0.91060	2.28417	0.91059	2.28414

This difference in divergence of the numerical solution from the saddle point can be utilized. Suppose that one has an initial value problem in which the initial data are given on the saddle curve itself at a point such as A in sketch (a); the problem is to integrate numerically across the saddle point and proceed along the same saddle curve. Suppose, further, that proceeding forward (increasing s) from A, one found, by experiment, results similar to those represented by curves AA' and AA''. It would appear, on the basis of the discussion in the previous paragraph, that one could readily solve the problem by iterating on results obtained by integrating backward from suitable guesses near the critical point (but still in the same half-plane as the initial point). This approach does not succeed in all cases; there are two conditions under which it either is not helpful or fails disastrously:

1. The eigenvalues σ_1 and σ_2 are equal in magnitude so that the integral curves are right hyperbolas and neither direction of approach to the saddle point is preferred.

2. Coupled into the equations are other eigenvalues that are relatively large negative numbers with respect to forward integration. These become large positive numbers when the direction of integration is reversed and lead to serious inherent instability.

It will be found that both the above conditions operate in the problem of non-equilibrium channel flow when passing through the throat section. Nevertheless, the saddle points that arise in the solution of the blunt-body problem by means of the method of integral relations do indeed approach their asymptotes at different rates. Thus the device mentioned above may be put to good use.

Some practical considerations.- If each of the quantities w and x in equations (16) is considered as a function of s (see eqs. (18)), then, for forward integration, the saddle point becomes the point at $s = +\infty$. The derivatives w' and x' approach zero as $s \to \infty$, as shown for w(s) in sketch (c). Care should be taken that too much calculation time is not wasted in indiscriminate attempts to integrate too close to the saddle point in terms of s.

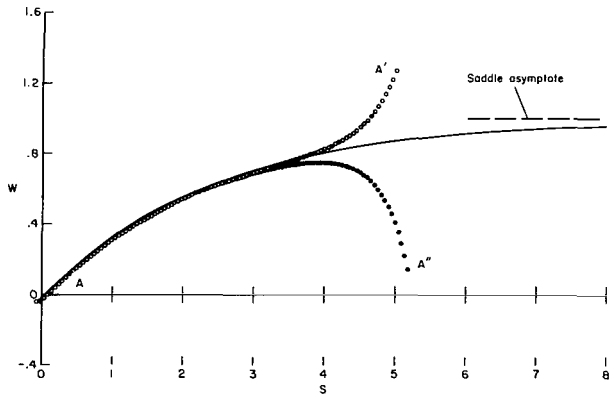

Sketch (c).- Saddle curve behavior in terms of independent variable s.

An extrapolation across the saddle point to obtain initial values from which the solution can be started again on the opposite side is often satisfactory. The extrapolation should be based on two integral curves that are initially very close and later diverge in opposite directions, such as curves AA' and AA" in sketch (a). To offset the inaccuracy inherent in such an extrapolation, notice that integral curves have the property that the direction of motion along the curve with increasing s reverses as the saddle point is crossed. Hence, by extrapolating past the saddle point, and reversing the sign of the increment Δs, an integral curve that approaches the saddle curve, rather than one diverging from it, will be obtained. This convergence will not occur if the saddle point is not passed in the extrapolation. For example, starting at point C in sketch (a) and integrating 134 steps with stepsize $\Delta s = h = -0.05$, the curve CC' was obtained. The end results are given in table III.

TABLE III

Curve	Initial values		Numerical results after 134 steps		Exact results at same s	
	w	x	w	x	w	x
CC'	1.2	2.6	2.0156	4.9518	2.0158	4.9523

A point on the saddle line itself occurs at $w = 4.9528$, $x = 2.0160$, so that, even with the "bad start" at C, the integration approaches (for this example) the desired saddle curve with good accuracy.

NUMERICAL CALCULATION OF EQUILIBRIUM FLOW

The equations for inviscid channel flow of a gas in chemical equilibrium have been given above (eqs. (1)). These equations were then put in autonomous form (eqs. (3)), and they will be treated in that form in the numerical work described below. In the following discussion of the numerical solution of equations (3), the eigenvalue structure at the throat is first considered. Then the integration process used to approach and pass through the saddle point at the throat of the channel is presented.

Conditions at the Throat

Although all solutions for equilibrium channel flows presented in this report are for a real gas in chemical equilibrium (carried out by means of the real-gas program described in ref. 6), it is instructive to inspect analytically the nature of the solution at the throat when perfect gas approximations are valid. This is because the eigenvalues (as determined numerically) at the throat, for the equilibrium real-gas flow, show a similarity with those determined analytically for a perfect gas.

Thus, consider the locally linearized equations for perfect-gas, channel flow right at the throat section where $\bar{A}_x = 0$ and $u = a = a^*$. The A matrix given by equation (12) simplifies to

$$[A] = \begin{bmatrix} 0 & 0 & 0 & -s_o a^{*3}\bar{A}_{xx} \\ 0 & 0 & 0 & s_o \rho a^{*2}\bar{A}_{xx} \\ 0 & 0 & 0 & s_o \rho a^{*4}\bar{A} \\ -2s_o a^*\bar{A} & -s_o \frac{1}{\rho} a^{*2}\bar{A} & s_o \frac{1}{p} a^{*2}\bar{A} & 0 \end{bmatrix} \tag{23}$$

Note that the only differences between this result and the corresponding one for a real gas appear in the elements a_{42} and a_{43}, where the terms $(\partial a^2/\partial \rho)_p$ and $(\partial a^2/\partial p)_\rho$ have been simplified in the present case of a perfect gas.

The eigenvalues of the matrix in equation (23) are given by the roots of the equation

$$\sigma^2\left[\sigma^2 - s_o{}^2\bar{A}\bar{A}_{xx}a^{*4}\left(\frac{\rho}{p} a^{*2} + 1\right)\right] = 0$$

After some reduction, using the relation $a^{*2} = a^2 = \frac{\gamma p}{\rho}$, the eigenvalues are found to be

$$\left.\begin{aligned} \left.\begin{matrix}\sigma_1 \\ \sigma_2\end{matrix}\right\} &= \pm\left[(\gamma + 1)\bar{A}\bar{A}_{xx}a^{*4}s_o^2\right]^{1/2} \\ \sigma_3 &= \sigma_4 = 0 \end{aligned}\right\} \tag{24}$$

The scaling factor s_o, still at our disposal, is taken to be

$$s_o = \frac{1}{a_o^2} \tag{25}$$

where a_o is the sound speed at $u = 0$, that is, under reservoir conditions. This is convenient because then

$$\frac{dx}{ds} = \frac{a^2 - u^2}{a_o^2}\bar{A} \approx \bar{A}$$

when $u \ll a$. In all cases considered in this report, the area variation is taken to be

$$\bar{A} = 1 + x^2 \tag{26}$$

With the above choices for s_o and $\bar{A}$, the nonzero eigenvalues become

$$\left.\begin{matrix}\sigma_1 \\ \sigma_2\end{matrix}\right\} = \pm\left[(\gamma + 1)2\,\frac{a^{*4}}{a_o^4}\right]^{1/2}$$

$$= \pm\left(\frac{8}{\gamma + 1}\right)^{1/2} \approx \pm 1.83 \tag{27}$$

when $\gamma = 1.4$. The eigenvalues at the throat in a perfect-gas flow therefore are real and of opposite sign. Hence, there is a saddle point at the throat, and the situation is one in which backward integration near (but not across) the saddle point becomes useless, as pointed out previously. The same situation is found when we deal with a real gas, where the eigenvalues are numerically determined.

Calculations Upstream and Downstream of the Throat

The channel flow equations in autonomous form, equations (3), were integrated numerically by means of the second-order Runge-Kutta procedure discussed above (eqs. (20)). The first case considered is one in which the approximate reservoir conditions are

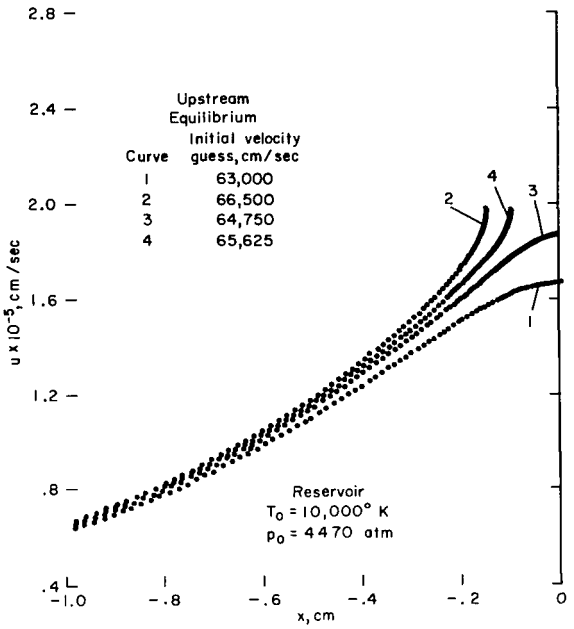

Sketch (d).- Integral curves near the saddle curve for a real gas flowing in equilibrium through a nozzle; reservoir conditions, equations (28a).

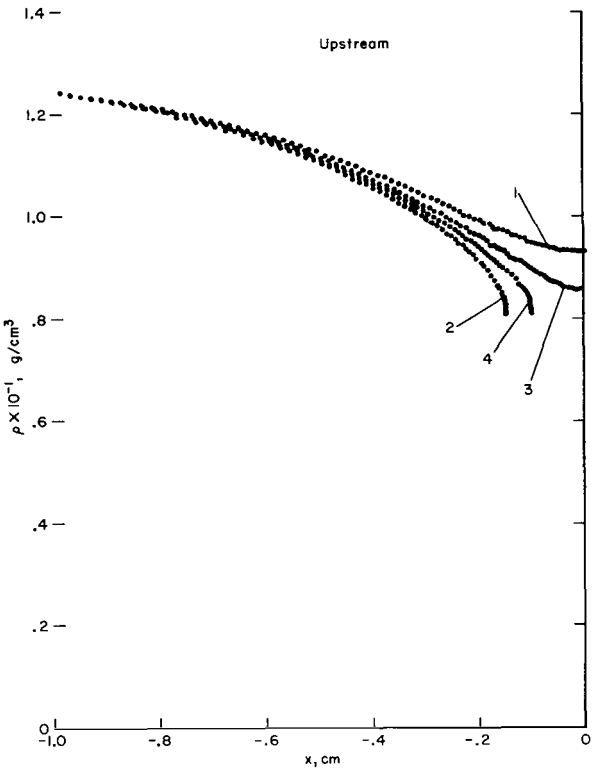

Sketch (e).- Integral curves near the saddle curve for a real gas flowing in equilibrium through a nozzle; reservoir conditions, equations (28a).

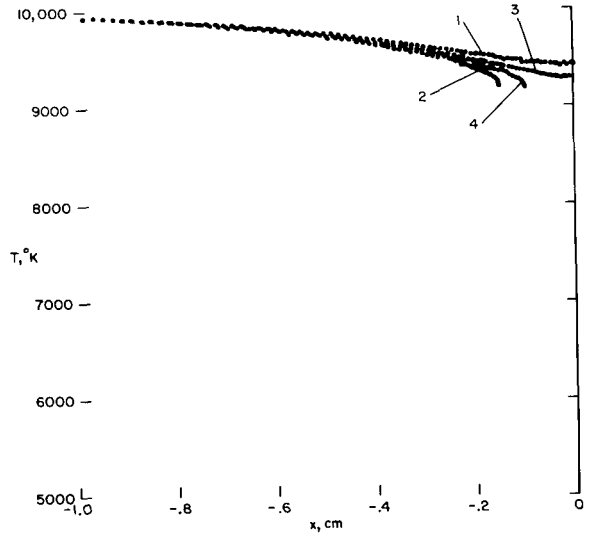

Sketch (f).- Integral curves near the saddle curve for a real gas flowing in equilibrium through a nozzle; reservoir conditions, equations (28a).

$$\left.\begin{aligned} T_o &= 10{,}000^\circ \text{ K} \\ p_o &= 4470 \text{ atm} \end{aligned}\right\} \qquad (28a)$$

Integration was begun at $x = -1.0$ cm, where the throat, for the channel shape given by equation (26), occurs at $x = 0$. Results for four guessed values of the initial velocity are shown in sketch (d). The saddle-point behavior near $x = 0$ shows clearly. Also, sketches (e) and (f) show the calculations of density ρ and temperature T corresponding to the initial guessed values of velocity. Many such curves can be calculated in a few seconds, and the computations can easily be automated. Thus, in the final program, such solutions are calculated until the saddle point is sufficiently well located,

an extrapolation is made across the saddle point, and the integration continued as far as required downstream, all in a single run. The final downstream variation of the physical quantities u, ρ, p, and T is shown in sketch (g). These results will be used later in comparisons to be made with calculations of nonequilibrium flow.

In support of the claim made above that the eigenvalues of the equilibrium real-gas flow calculations are analogous to those for a perfect-gas flow, sketch (h) shows the eigenvalues actually calculated (for reservoir conditions (28a)) as functions of distance x along the channel. It is seen that, indeed, when x = 0, two of the eigenvalues vanish and the remaining two are equal in magnitude and of opposite sign. (The magnitude of the eigenvalues is 2.0 rather than 1.83.) In this sketch, only the real part of the complex eigenvalues is shown (all complex eigenvalues appear as conjugate complex pairs since the elements of the matrix [A] are real). The maximum magnitude of any eigenvalue is less than 6 in this case, so a step size $h = \Delta s = 0.02$ is well within the stability boundary ($|\sigma h| < 2$) for the integration method used. At no stage of the calculations were any of the eigenvalues pure imaginary, for which the Runge-Kutta second-order method is unstable (see ref. 5, p. 83). Hence the explicit equations (20) were adequate for solution throughout the entire range.

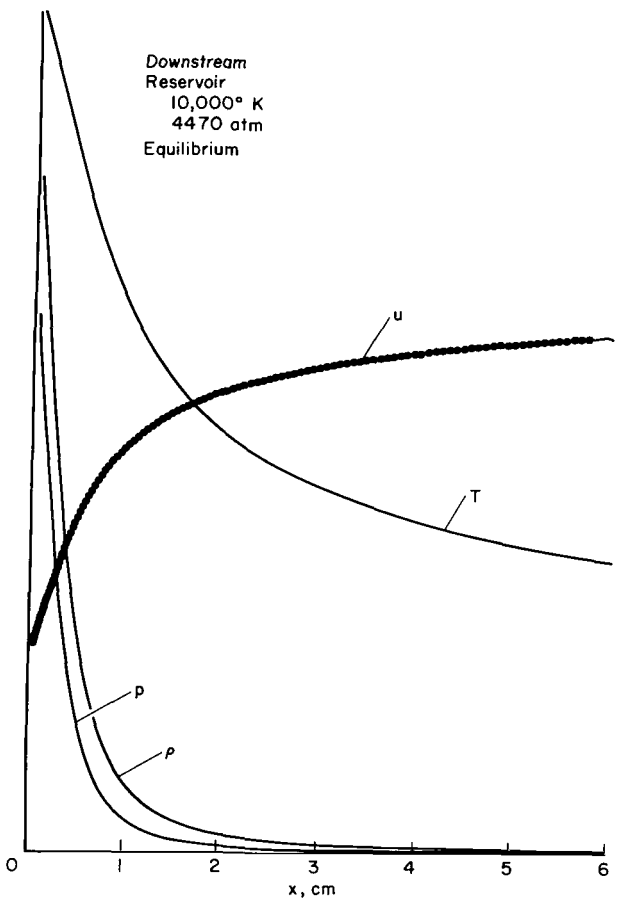

Sketch (g).- Channel flow solution for a real gas in equilibrium downstream from the throat of a nozzle; reservoir conditions, T_o = 10,000° K, p_o = 4470 atmospheres.

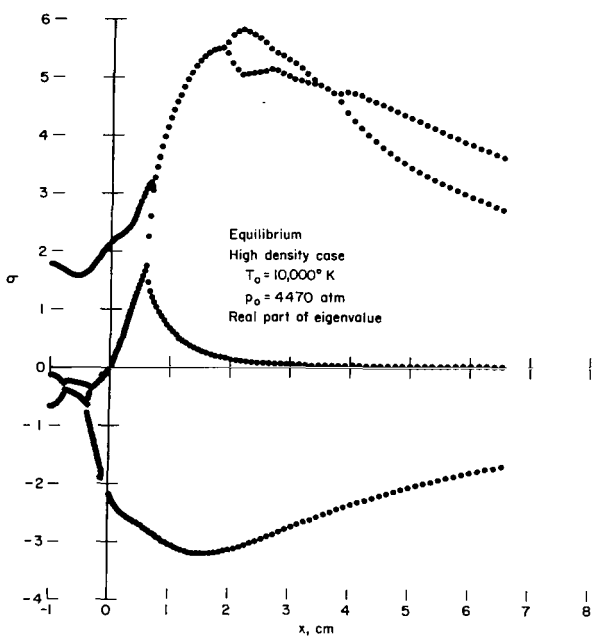

Sketch (h).- Local eigenvalues in the equations representing the channel flow of a real gas in equilibrium flowing through a nozzle; reservoir conditions, T_o = 10,000° K, p_o = 4470 atmospheres.

The eigenvalue patterns for two other solutions, corresponding to assumed equilibrium channel flow with reservoir conditions

$$\left.\begin{aligned} T_o &= 8{,}000^\circ \text{ K} \\ p_o &= 100 \text{ atm} \end{aligned}\right\} \tag{28b}$$

and

$$\left.\begin{aligned} T_o &= 10{,}000^\circ \text{ K} \\ p_o &= 0.2 \text{ atm} \end{aligned}\right\} \tag{28c}$$

are shown in sketches (i) and (j). The scaling (factor s_o in eqs. (3)) was chosen so that the right side of equation (3d) was 1 at the beginning of the integration. It is interesting to note that in spite of the large difference in reservoir pressures (0.2 to 4470 atm), the eigenvalue curves are much alike in shape and magnitude in the three cases. The nonequilibrium real-gas flow for the same three sets of reservoir conditions is examined in the next section.

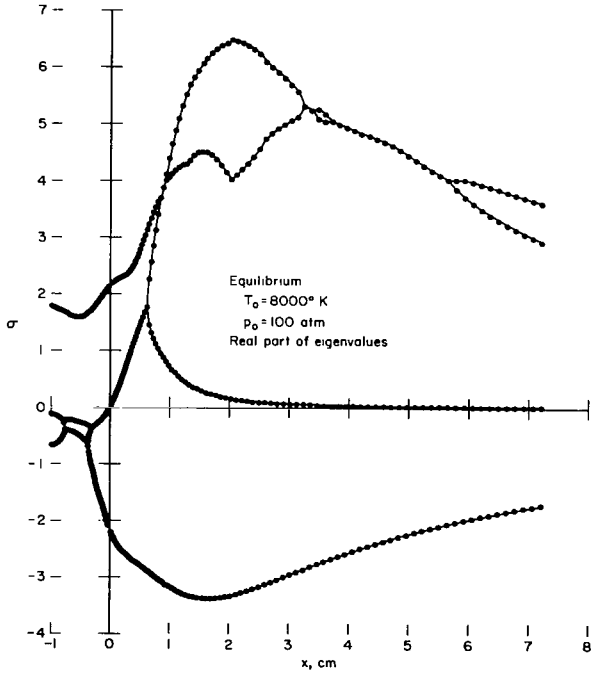

Sketch (i).- Local eigenvalues in the equations representing the channel flow of a real gas in equilibrium flowing through a nozzle; reservoir conditions, T_o = 8000° K, p_o = 100 atmospheres.

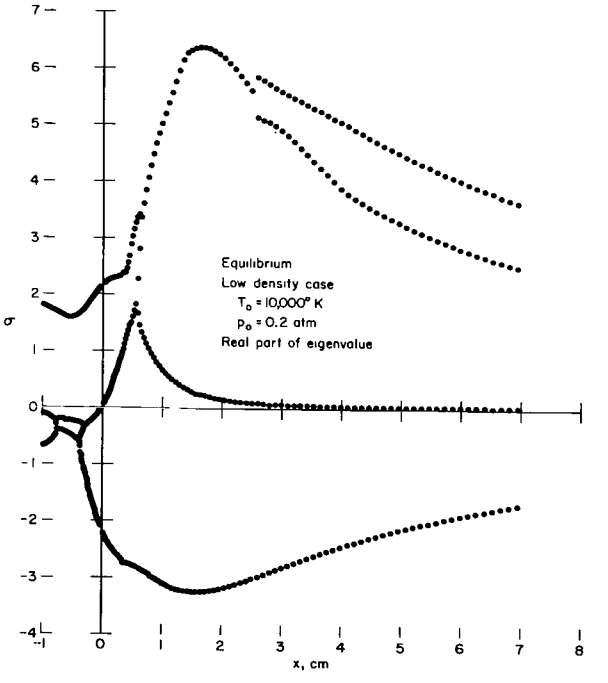

Sketch (j).- Local eigenvalues in the equations representing the channel flow of a real gas in equilibrium flowing through a nozzle; reservoir conditions, T_o = 10,000° K, p_o = 0.2 atmospheres.

NUMERICAL CALCULATION OF NONEQUILIBRIUM FLOW

Introduction

A variety of problems can arise when one seeks to make numerical calculations of a gas flowing out of chemical equilibrium. Some of these are discussed in the following. The problem of providing a suitable mathematical model is not considered here; we use the same model as that described in reference 2, which, in turn, was taken from references 7 and 8. There is no essential difficulty in casting the equations in finite-difference form. In fact, there is little numerical difficulty in constructing the $[A_n]$ matrix (see eq. (13)) if it is required. The real difficulties are more fundamental. For example, the saddle-point problem still occurs in the throat region, and, if treated in the way outlined above, requires an extrapolation of all nine species across the critical point (which is no longer exactly at the minimum section). In addition, the problem of parasitic eigenvalues (numerically large negative eigenvalues which, for numerical stability, force an unnaturally small step size, see ref. 2) can now arise. Furthermore, these parasitic eigenvalues appear near the beginning of the calculations (i.e., in the throat section) rather than downstream as is the case in the study of nonequilibrium flow behind shocks.

The above difficulties can be compounded in some calculations when the gas is very nearly in equilibrium, because, in such a case, the Q^1 in equations (4) and (5) are composed of terms formed by the product of very small and very large terms (indeterminate forms in the mathematical model when the equilibrium limit is approached). Surprisingly, this near indeterminacy appeared to cause no trouble in any of the calculations carried out. This matter is reserved for discussion in the last section after the results have been presented.

Parasitic Eigenvalues

It is well known that the equations representing a gas flowing in chemical equilibrium have local parasitic eigenvalues. That is, some of the eigenvalues of the $[A_n]$ matrix (found by putting eqs. (5) in the form of eq. (10)) are very large negative numbers compared to others that determine the solution.[1] In flows from nozzles with high reservoir pressures, these parasitic eigenvalues appear upstream of the throat.

Some of the eigenvalues for flow from the reservoir conditions given in equation (28a) are shown[2] in figure 1. Actually, several large negative eigenvalues are contained in the local $[A_n]$ matrix. The three largest ones are shown in the figure. Now it should be mentioned that, for these reservoir conditions, the gas in the nozzle between the reservoir and a section about

[1]These eigenvalues, which determine the solution, are called driving eigenvalues.

[2]Notice the numerical evidence of singular behavior at the critical point.

3 cm downstream from the throat is very nearly in equilibrium. This can be shown by comparing solutions for a nonequilibrium case with those for an equilibrium one (fig. 2). In this region of near equilibrium, the eigenvalues that are actually driving the solution are those already shown in sketch (h), two of which are also included in figure 1 for comparison. This extreme difference (about 1×10^7) between the largest negative eigenvalues and the driving eigenvalues forces one, practically speaking, to an implicit numerical integration method.

As in reference 2, equations (5) were converted to equations (10) by calculating the elements $(a_{ij})_n$ numerically, that is, by using equation (13). The modified Euler implicit differencing scheme

$$w_{n+1} = w_n + \frac{1}{2}h\left(w'_{n+1} + w'_n\right) \tag{30}$$

was used, leading to the formula

$$\left([I] - \frac{1}{2}h[A_n]\right)\left(\vec{w}_{n+1} - \vec{w}_n\right) = h\vec{F}_n + O(h^3) \tag{31}$$

Calculations were started at $x = -1$ cm, and all integrations were carried out with s as the independent variable. Although the product of the step size and the largest negative eigenvalue started as high as -8000, the results were satisfactory, as illustrated in figure 2, where the nonequilibrium calculations are compared with the previously discussed equilibrium ones. The equilibrium species concentrations shown in figure 2(b) are readily calculated for the given reservoir composition from the assumption of chemical equilibrium and knowledge of two thermodynamic variables, say, density ρ and temperature T as shown in figure 2(a).

The saddle-point problem was treated exactly as in the equilibrium case by finding two integral curves that diverged to opposite sides of the critical point. The results for ρ, u, and T are shown in sketches (k), (ℓ), and (m). Extrapolation across the saddle point was carried out for the velocity, density, and temperature. The individual species were also extrapolated, but the downstream calculations appeared to be sensitive to small changes ("errors") in the species concentrations; hence, for the results shown, only the velocity, density, and temperature were extrapolated, and the species concentrations were chosen to be those in exact equilibrium with the extrapolated temperature and density.

Sketches (k) and (ℓ) also show the result of "bad" extrapolation; that is, the circled points are the results of calculations made with deliberate errors in the extrapolations for ρ, u, and T (these correspond to the example of the curve marked CC' in sketch (a)). In this case, the convergence of the integral curves to the saddle curve is evident. No cases to the contrary were found, although no "extreme" errors were tried.

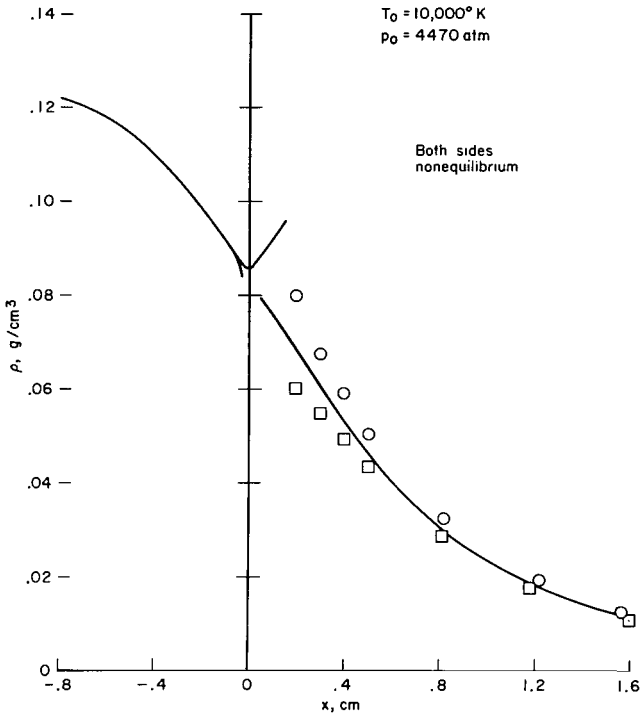

Sketch (k).- Integral curves near the saddle curve for a real gas in nonequilibrium flow through a nozzle; reservoir conditions, T_o = 10,000° K, p_o = 4470 atmospheres.

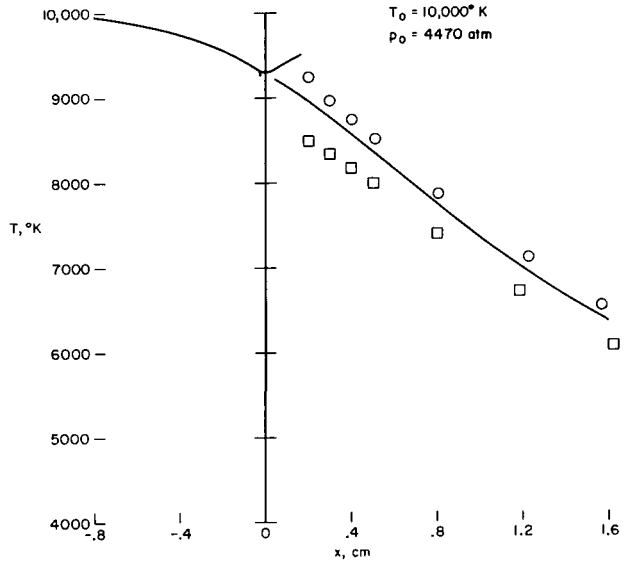

Sketch (m).- Integral curves near the saddle curve for a real gas in nonequilibrium flow through a nozzle; reservoir conditions, T_o = 10,000° K, p_o = 4470 atmospheres.

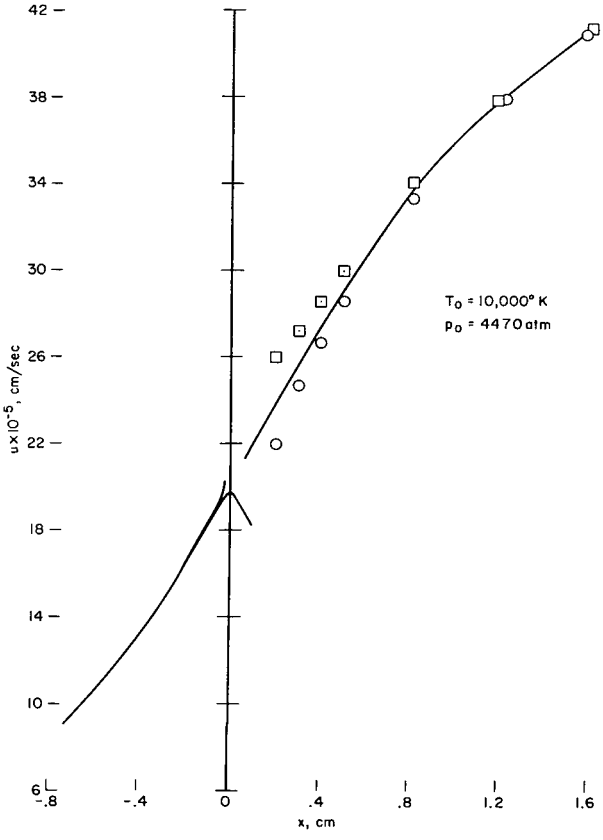

Sketch (ℓ).- Integral curves near the saddle curve for a real gas in nonequilibrium flow through a nozzle; reservoir conditions, T_o = 10,000° K, p_o = 4470 atmospheres.

The eigenvalues for the two lower pressure reservoirs, given in equations (28b) and (28c), as well as the solutions for the nonequilibrium flow through the nozzle region under these conditions, are shown in figures 3 through 6. The parasitic eigenvalues tend to disappear as the reservoir pressure drops, and, in fact, in the lowest pressure case they have, for practical purposes, vanished. The latter case, therefore, can be integrated all the way from x = -1 using the explicit method defined in equation (20).

Notice that for the conditions given in equation 28(c) (low reservoir pressure) the nozzle is out of equilibrium well upstream of the

minimum section. In this case, all of the species, as well as the velocity and thermodynamic variables, had to be extrapolated across the saddle point. For these conditions, however, this procedure appears to give quite satisfactory values as the results shown in figure 6 indicate by their smoothness.

Calculations Made Near Equilibrium

As mentioned in the introduction to this section, some special problems arise when the flow is nearly in equilibrium, due to a numerical indeterminacy in the species production Q^i (see eqs. (4)). This indeterminacy arises in the the product of X_i, the "degree of nonequilibrium," (ref. 7) $X_i \to 0$ as equilibrium is approached. For example, a typical X_i, for the reaction $N_2 \rightleftarrows 2N$, is given by

$$X_2 = \frac{1 - \rho\gamma_2^2}{\gamma_5 K_2} \qquad (32)$$

where K_2 is the equilibrium constant for the reaction specified.

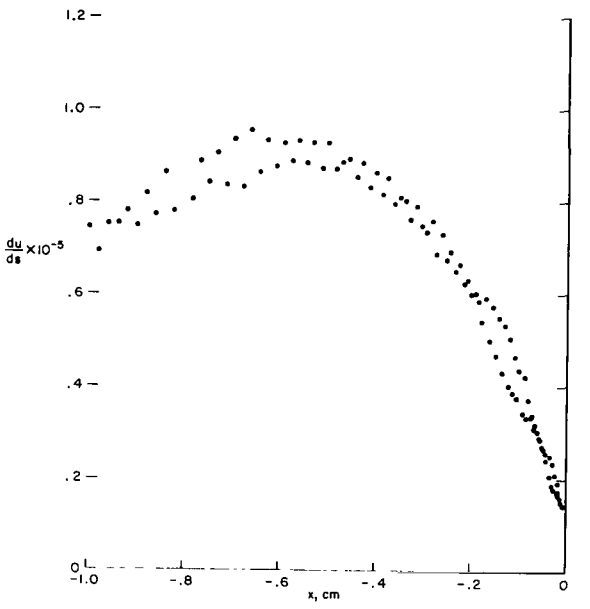

Sketch (n).- The fluctuation of du/ds in calculations made very near equilibrium; upstream from nozzle.

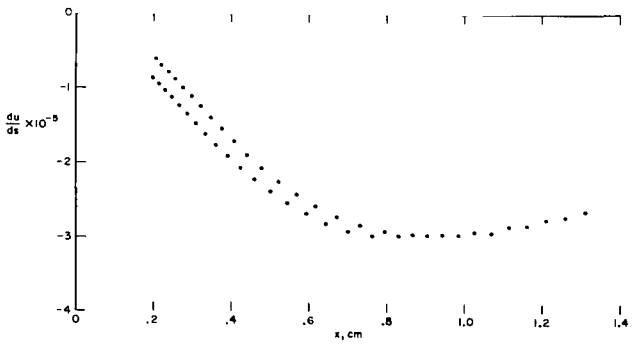

Sketch (o).- The fluctuation of du/ds in calculations made very near equilibrium; downstream from nozzle.

All computations were made in 8-place (27-bit) floating-point arithmetic, and in the numerical calculations under near equilibrium conditions the subtractions needed to form the X_i (e.g., eq. (32)) lost some of the significant figures. Although a quantitative analysis of the processes involved has not been carried out, the numerical evidence indicated that the loss was not disastrous. It is thought that this is due to the fact that the product of step size and driving eigenvalues was sufficiently small that valid information was obtained from whatever significant figures remained. At any rate, sufficient information was retained to provide the accuracy indicated in figure 2 for the high-pressure reservoir conditions (28a) and the flow model implicit in equations (5).

In near equilibrium calculations, most of the derivatives fluctuated within a band on successive steps. For example, typical results for du/ds on the upstream and downstream side of the throat are shown in sketches (n) and (o). This kind of behavior for the derivative terms is typical of the unconditionally stable

implicit methods when they are being used in the presence of large negative eigenvalues. The following is offered as an explanation:

1. The solution to the difference equations (in linearized form, at least) depends upon the sum of a number of terms represented (for the implicit modified Euler method) by

$$C_k\left[\frac{1 + \frac{1}{2} h\sigma_k}{1 - \frac{1}{2} h\sigma_k}\right]^n$$

where n is step number, σ_k is an eigenvalue in $[A_n]$, and C_k is a constant that depends on the initial conditions.

2. If $h\sigma_k$ is negative, the magnitude of the term in brackets is always less than 1, but if $h\sigma_k$ is a large negative number, the magnitude of the term within brackets is not much less than 1, and, furthermore, it is always negative.

3. In effect, then, the solution of the difference equation is composed of two kinds of terms. For example,

$$w = \overbrace{C_o(0.021\ldots)^n + C_1(-0.035\ldots)^n + \ldots}^{\text{driving terms}}$$

$$\overbrace{+ C_k(-0.999\ldots)^n + C_{k+1}(-0.999\ldots)^n + \ldots}^{\text{parasitic terms}}$$

4. The terms $(-0.999\ldots)^n$ oscillate between $+1$ and -1 as n is even or odd and if the coefficients C_k, C_{k+1}, . . . are not exactly zero (they cannot be exactly zero in truncated floating-point arithmetic). This will appear as "noise" at some level of significance in the numerical solution.

5. Apparently, for the mathematical model chosen and for the arithmetic used to study it, this noise is just below the level of usable information in the values of the dependent variables at near equilibrium conditions.

When calculations were made even slightly away from equilibrium, the fluctuations (to the scale shown) disappeared and the numerical calculations appeared "normal." For example, the transition from fluctuating to relatively smooth values of the derivative du/ds is seen in sketch (o) to occur about 1 cm after passing the minimum section in the high pressure case. To the scale used in figure 1, the gas is not yet out of equilibrium until about 3 cm downstream from the throat.

CONCLUDING REMARKS

For problems that require the numerical integration of differential equations through a saddle-point type of singularity, it is necessary (1) to identify the location of the saddle point and then (2) to use special numerical techniques to obtain the solution of the differential equations in the saddle-point vicinity. If the eigenvalues of the system having different sign are also of different magnitude, the technique of backward integration, that is, integration from the saddle-point vicinity outward, may be useful.

Large parasitic eigenvalues may be present in the numerical integration of the differential equations governing the flow of a gas out of chemical equilibrium. In the model chosen, this was particularly true near the throat of the nozzle, and the severity of the parasitic behavior increased with increasing density. Use of an implicit numerical method is recommended for the most severe cases.

Ames Research Center
National Aeronautics and Space Administration
Moffett Field, Calif., 94035, Jan. 6, 1969
129-01-02-05-00-21

REFERENCES

1. Liepmann, H. W.; and Roshko, A.: Elements of Gasdynamics. John Wiley and Sons, Inc., New York, 1957.

2. Lomax, Harvard; and Bailey, Harry E.: A Critical Analysis of Various Numerical Integration Methods for Computing the Flow of a Gas in Chemical Nonequilibrium. NASA TN D-4109, 1967.

3. Hurewicz, Witold: Lectures on Ordinary Differential Equations. John Wiley and Sons, Inc., New York, 1958.

4. Fox, L. (Ed.): Numerical Solution of Ordinary and Partial Differential Equations. Pergamon Press, New York, 1962.

5. Lomax, Harvard: An Operational Unification of Finite Difference Methods for the Numerical Integration of Ordinary Differential Equations. NASA TR R-262, 1967.

6. Inouye, Mamoru; Rakich, John; and Lomax, Harvard: A Description of Numerical Methods and Computer Programs for Two-Dimensional and Axisymmetric Supersonic Flow Over Blunt-Nosed and Flared Bodies. NASA TN D-2970, 1965.

7. Marrone, Paul V.: Inviscid, Nonequilibrium Flow Behind Bow and Normal Shock Waves. Parts I and II. Cornell Aero. Lab. Rep. CAL-QM-1626-A-12, 1963.

8. Hall, J. G.; Eschenroeder, A. Q.; and Marrone, P. V.: Inviscid Hypersonic Airflows With Coupled Nonequilibrium Processes. Cornell Aero. Lab. Rep. CAL AF-1413-A-2, May 1962.

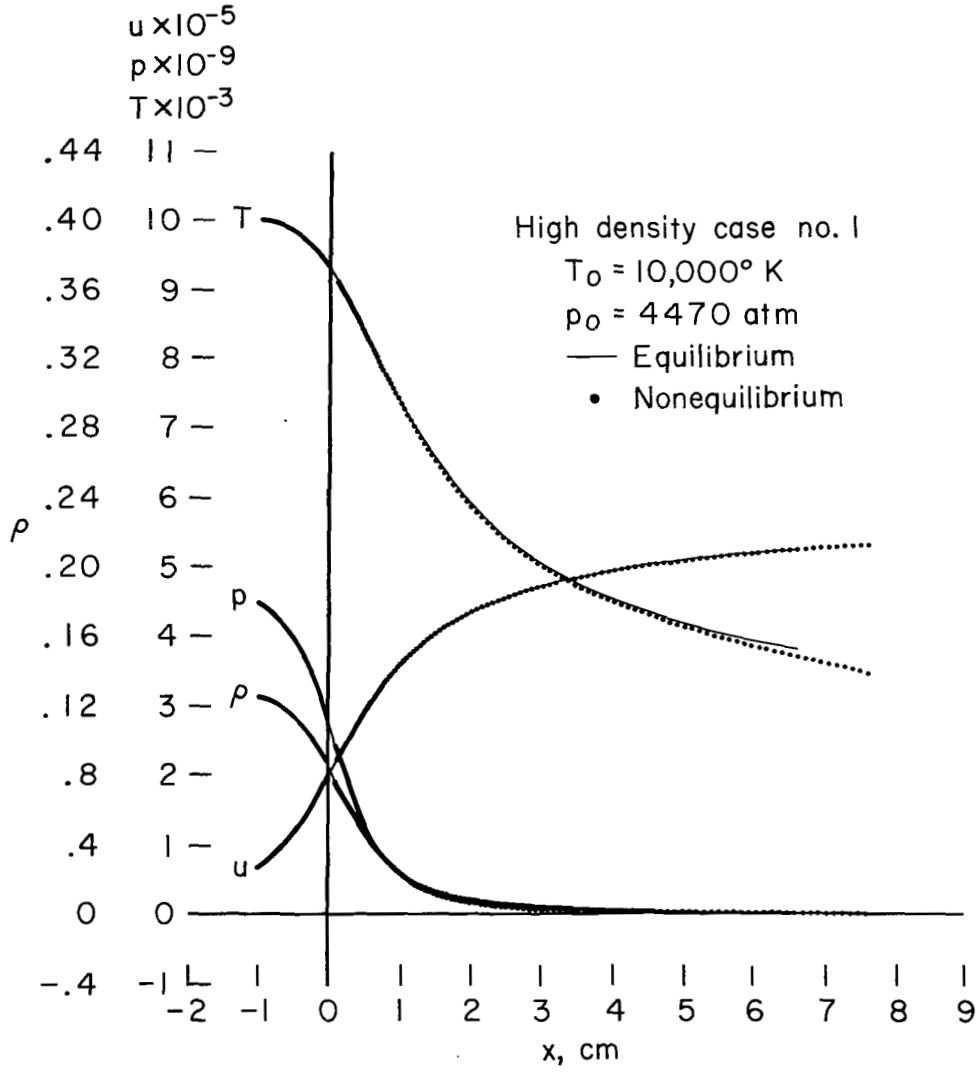

(a) Thermodynamic variables.

Figure 2.- Solution for the flow through a nozzle of a real gas in nonequilibrium; T_o = 10,000° K, p_o = 4470 atmospheres.

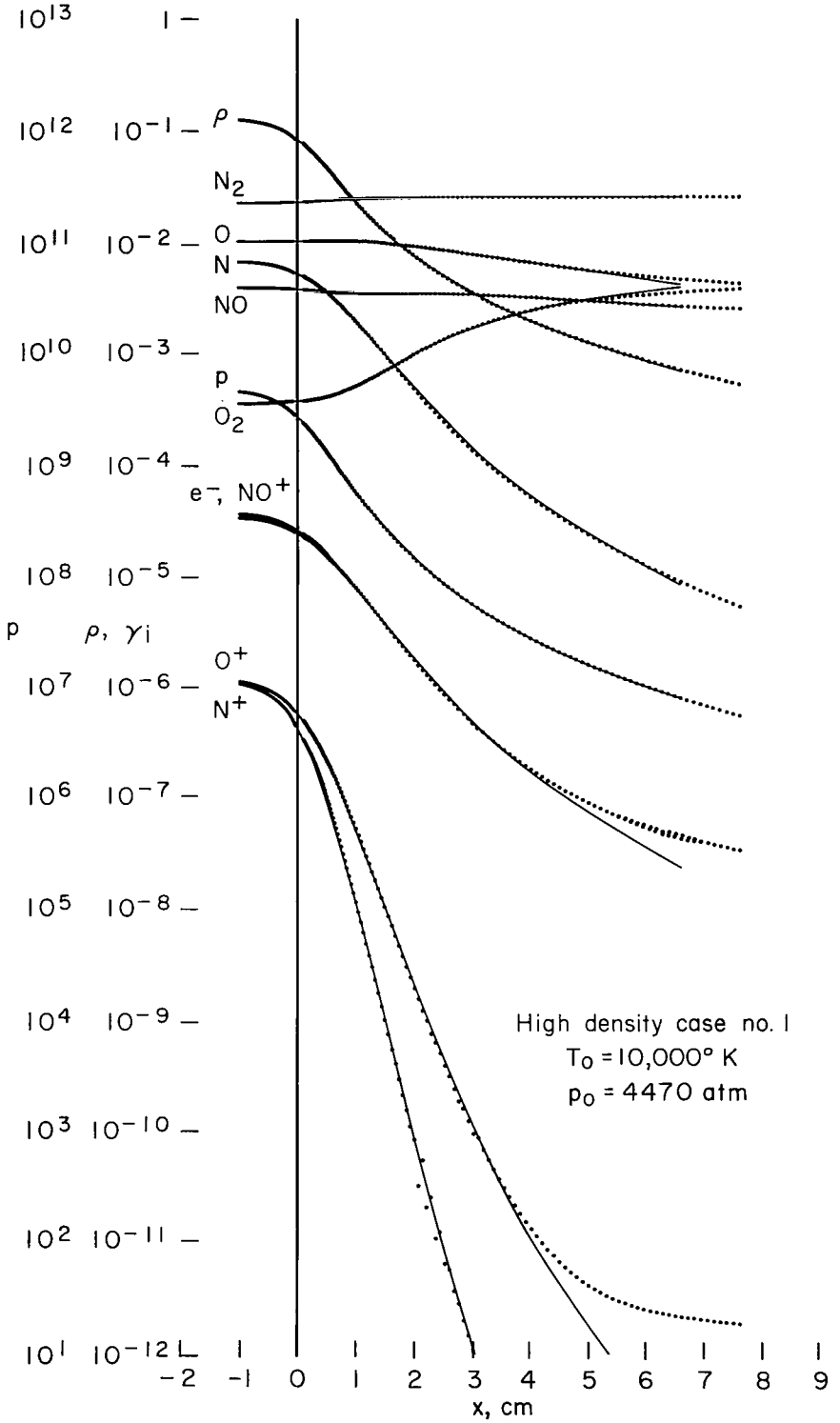

(b) Species concentrations.

Figure 2.- Concluded.

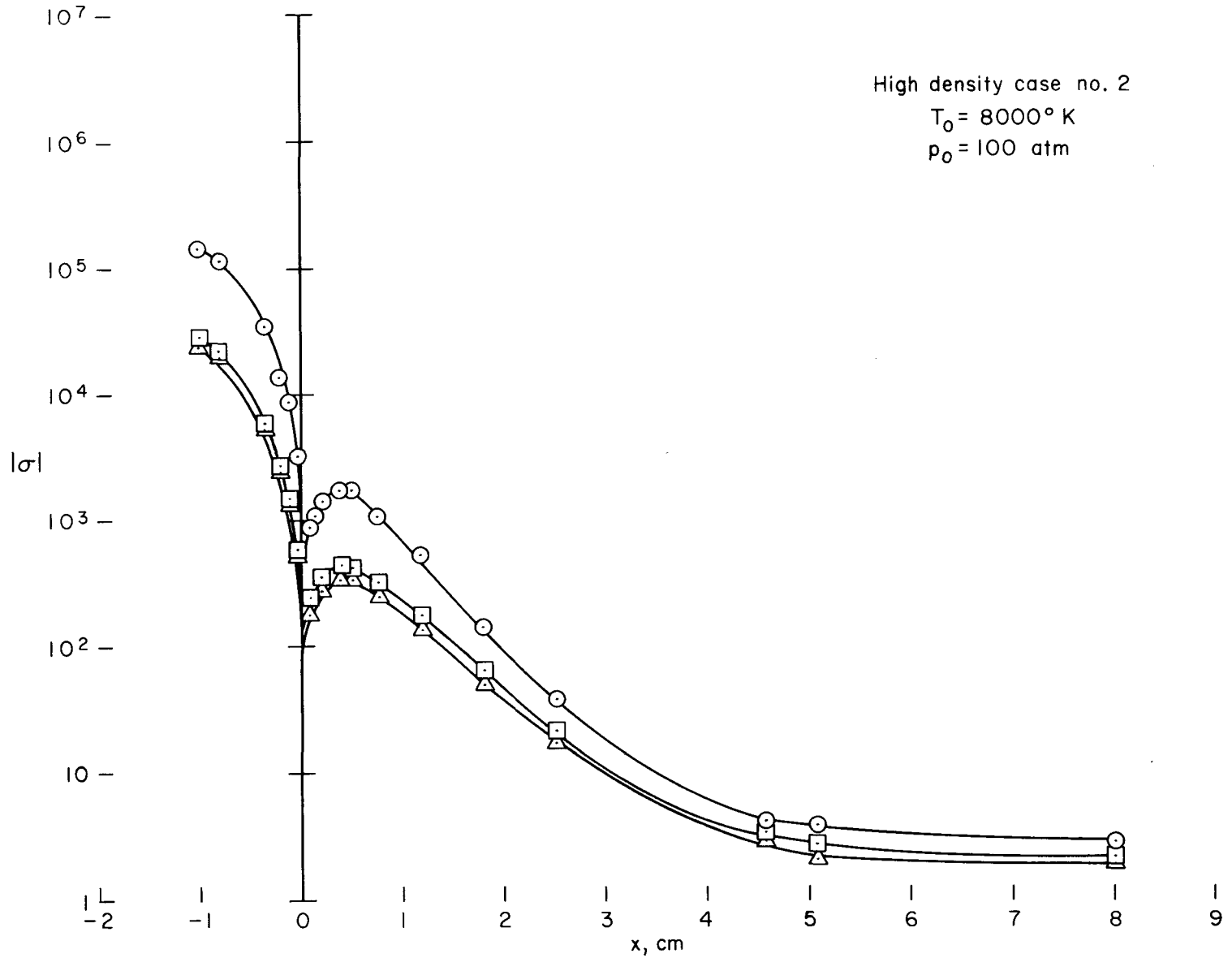

Figure 3.- Local eigenvalues in the equations representing the flow through a nozzle of a real gas in nonequilibrium; reservoir conditions, T_o = 8000° K, p_o = 100 atmospheres.

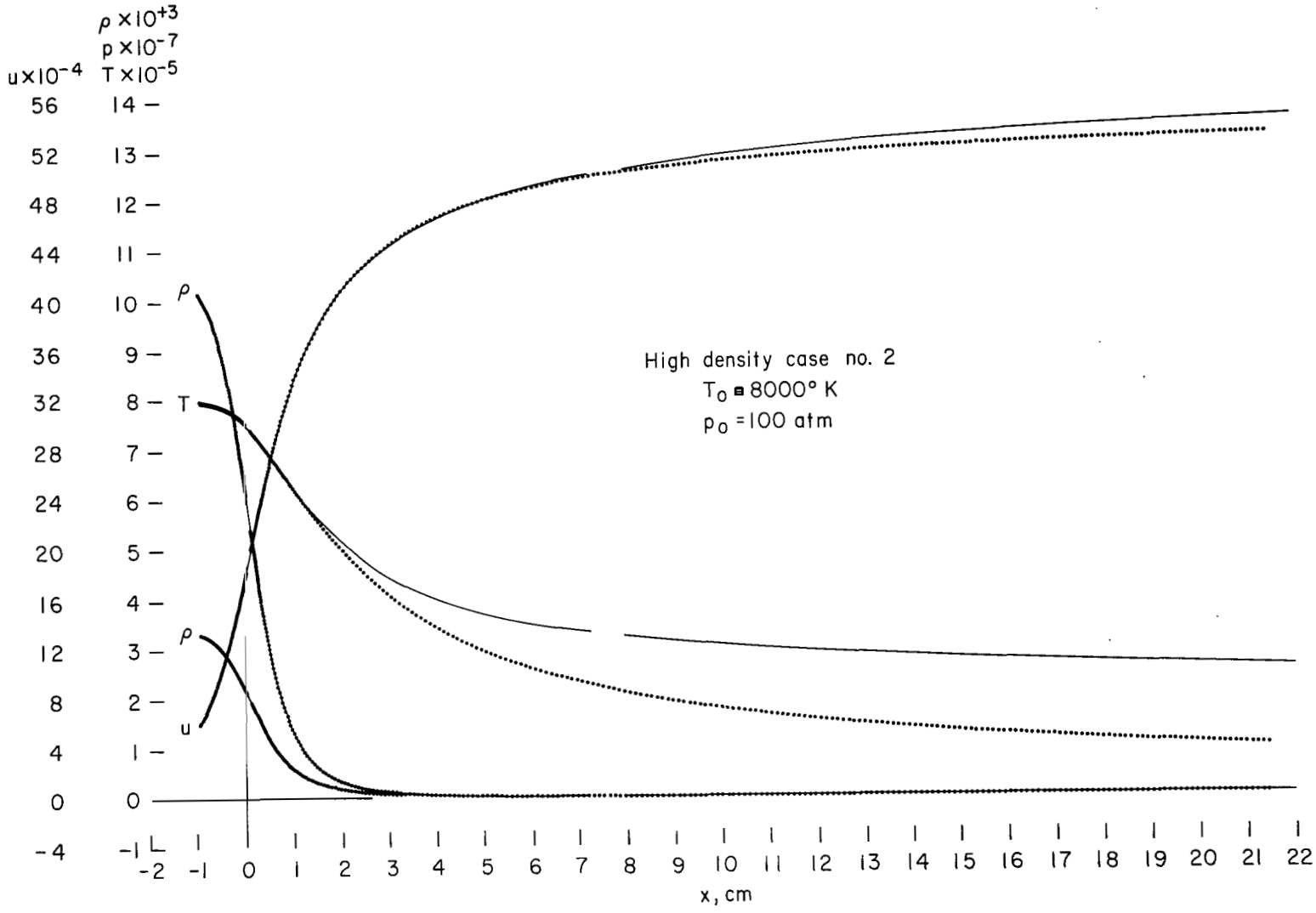

(a) Thermodynamic variables.

Figure 4.- Solution for the flow through a nozzle of a real gas in nonequilibrium; T_o = 8000° K, p_o = 100 atmospheres.

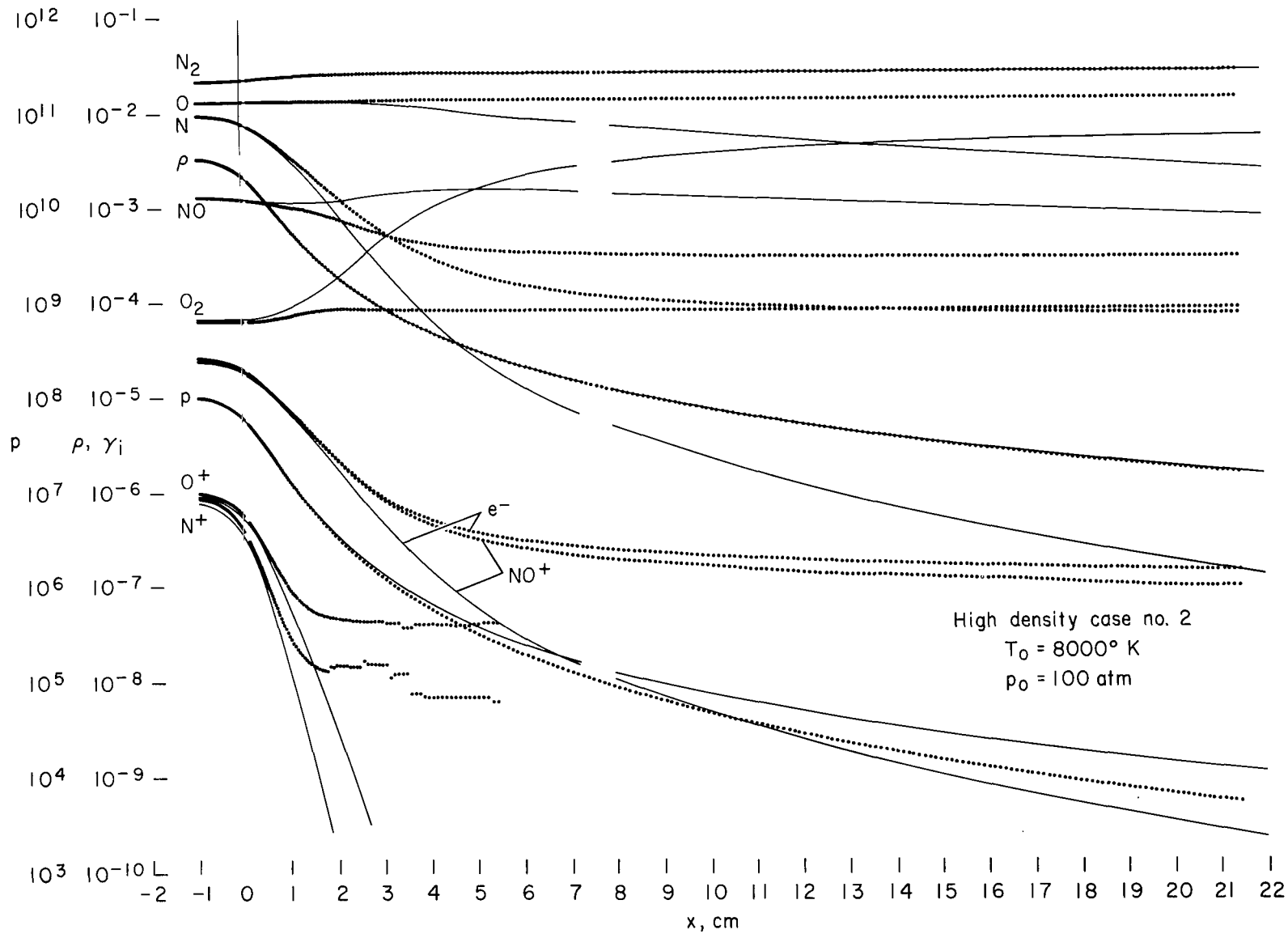

(b) Species concentrations.

Figure 4.- Concluded.

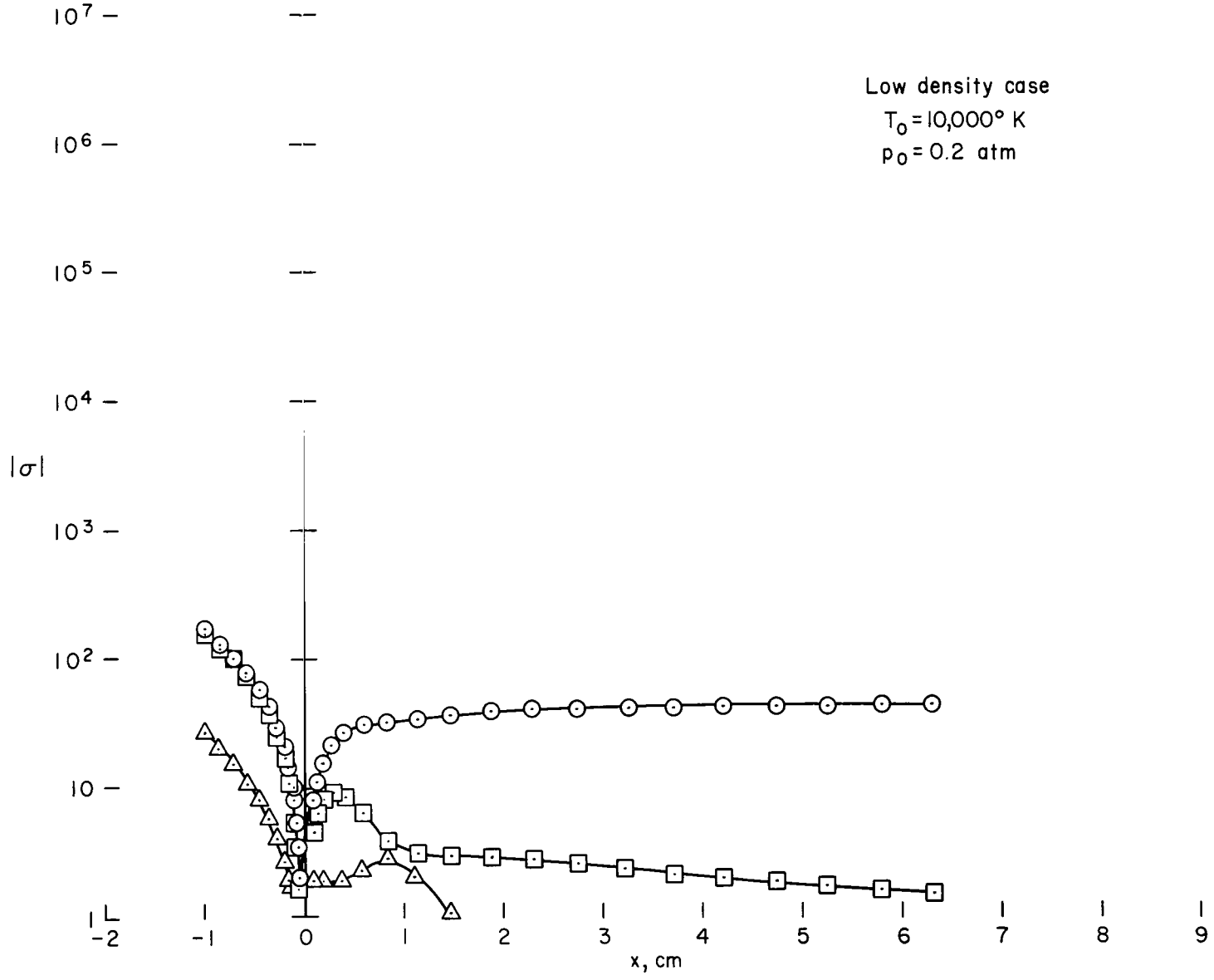

Figure 5.- Local eigenvalues in the equations representing the flow through a nozzle of a real gas in nonequilibrium; reservoir conditions, T_o = 10,000° K, p_o = 0.2 atmosphere.

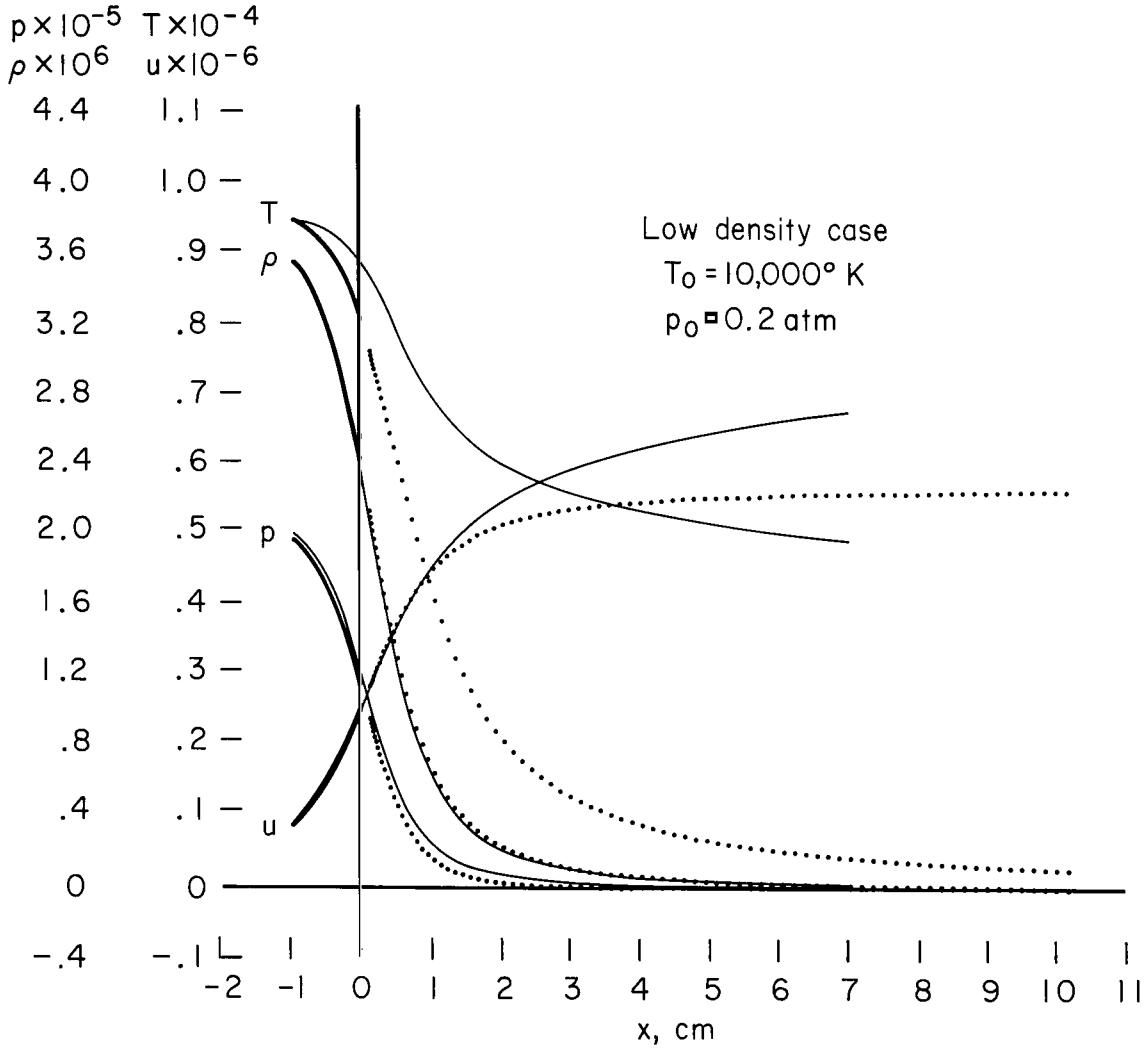

(a) Thermodynamic variables.

Figure 6.- Solution for the flow through a nozzle of a real gas in nonequilibrium; T_o = 10,000° K, p_o = 0.2 atmosphere.

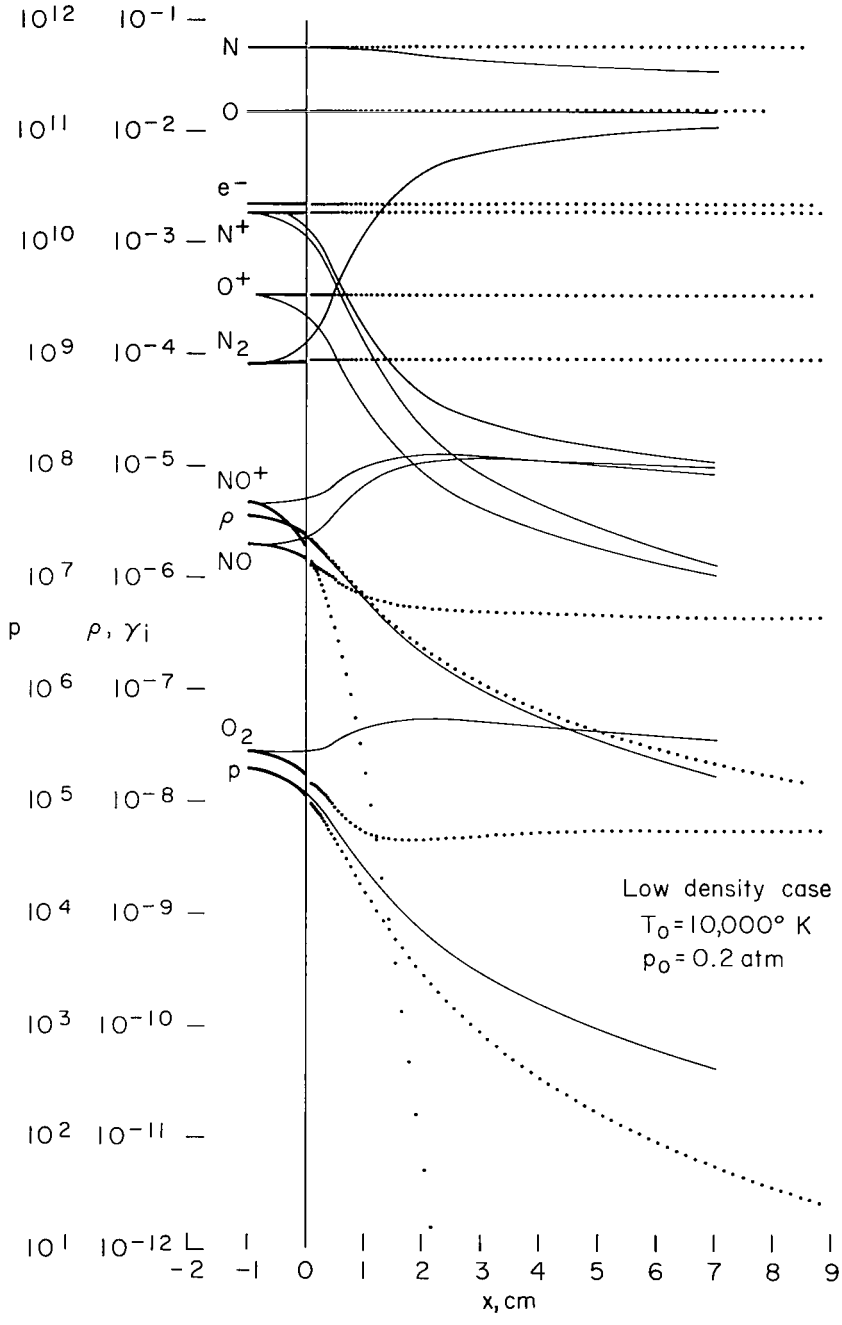

(b) Species concentrations.

Figure 6.- Concluded.

NATIONAL AERONAUTICS AND SPACE ADMINISTRATION
WASHINGTON, D. C. 20546

OFFICIAL BUSINESS

FIRST CLASS MAIL

POSTAGE AND FEES PAID
NATIONAL AERONAUTICS AND
SPACE ADMINISTRATION

POSTMASTER: If Undeliverable (Section 158 Postal Manual) Do Not Return

"The aeronautical and space activities of the United States shall be conducted so as to contribute . . . to the expansion of human knowledge of phenomena in the atmosphere and space. The Administration shall provide for the widest practicable and appropriate dissemination of information concerning its activities and the results thereof."

—NATIONAL AERONAUTICS AND SPACE ACT OF 1958

NASA SCIENTIFIC AND TECHNICAL PUBLICATIONS

TECHNICAL REPORTS: Scientific and technical information considered important, complete, and a lasting contribution to existing knowledge.

TECHNICAL NOTES: Information less broad in scope but nevertheless of importance as a contribution to existing knowledge.

TECHNICAL MEMORANDUMS: Information receiving limited distribution because of preliminary data, security classification, or other reasons.

CONTRACTOR REPORTS: Scientific and technical information generated under a NASA contract or grant and considered an important contribution to existing knowledge.

TECHNICAL TRANSLATIONS: Information published in a foreign language considered to merit NASA distribution in English.

SPECIAL PUBLICATIONS: Information derived from or of value to NASA activities. Publications include conference proceedings, monographs, data compilations, handbooks, sourcebooks, and special bibliographies.

TECHNOLOGY UTILIZATION PUBLICATIONS: Information on technology used by NASA that may be of particular interest in commercial and other non-aerospace applications. Publications include Tech Briefs, Technology Utilization Reports and Notes, and Technology Surveys.

Details on the availability of these publications may be obtained from:

SCIENTIFIC AND TECHNICAL INFORMATION DIVISION

NATIONAL AERONAUTICS AND SPACE ADMINISTRATION

Washington, D.C. 20546